

Second-order resonant Raman spectra of single-walled carbon nanotubes

S. D. M. Brown, P. Corio, and A. Marucci

Department of Physics, Massachusetts Institute of Technology, Cambridge, Massachusetts 02139

M. A. Pimenta

Departamento de Física, Universidade Federal de Minas Gerais, Caixa Postal 702, 30123-970 Belo Horizonte, Brazil

M. S. Dresselhaus

Department of Electrical Engineering and Computer Science and Department of Physics, Massachusetts Institute of Technology, Cambridge, Massachusetts 02139

G. Dresselhaus

Francis Bitter Magnet Laboratory, Massachusetts Institute of Technology, Cambridge, Massachusetts 02139

(Received 24 May 1999; revised manuscript received 26 August 1999)

An analysis of the second-order resonant Raman spectra of single-walled carbon nanotubes using different laser energies in the range 1.58–2.71 eV is presented. Major emphasis is given to the overtones and combination modes associated with the two dominant features of the first-order spectra, the radial breathing mode and the tangential mode. Both of these modes, as well as their second-order counterparts, are associated with resonant enhancement phenomena arising from electron-phonon coupling to the unique one-dimensional density of electronic states for the single-wall carbon nanotubes.

I. INTRODUCTION

The second-order Raman spectra of single-wall carbon nanotubes are unique relative to other crystalline systems in exhibiting features associated with resonant enhancement phenomena arising from the unique one-dimensional (1D) density of electronic states for carbon nanotubes. These second-order spectra are therefore selective of specific carbon nanotubes, just as it occurs for the first-order spectra.^{1–3} This paper focuses on the unique behavior of overtones and combination modes in the second-order Raman spectra associated with the dominant features in the first-order spectra, which exhibit strong resonant coupling to the 1D density of electronic states. Other features in the second-order spectra, not associated with the 1D resonant Raman scattering process, are briefly summarized here but are reported in detail elsewhere.⁴

Figure 1 shows the first-order and second-order features in the Raman spectra for single-wall carbon nanotubes over a broad range of phonon frequencies for three laser excitation energies E_{laser} . Since the relative intensities of the various features in Fig. 1 are dependent on the laser excitation energy, resonant Raman effects are as important in the analysis of the second-order spectra as they are for interpreting the first-order spectra.

The origin of the unique behavior of the second-order resonant Raman processes follows from the well-established features in the first-order spectrum of single-wall carbon nanotubes, which are directly related to the 1D density of electronic states shown in Fig. 2 for $\gamma_0 = 3.0$ eV,¹ where γ_0 is the nearest neighbor carbon-carbon overlap energy.⁶ Since prior plots of the energies for the van Hove singularities¹ were made at much too low a value of γ_0 to fit our experi-

mental results, Fig. 2 is useful for explaining the Raman spectra reported in this paper.

The two dominant features in the first-order Raman spectra for single-wall carbon nanotubes (see Fig. 1) are the radial breathing modes (located in the 150–200- cm^{-1} range) and the tangential modes (located in the 1530–1610- cm^{-1} range). Both of these features in the first-order Raman spectra are resonantly enhanced when the laser excitation energy (E_{laser}) is equal to the energy separation between a singularity in the 1D electron density of states in the valence and conduction bands, such as the E_{ii} energy separations (be-

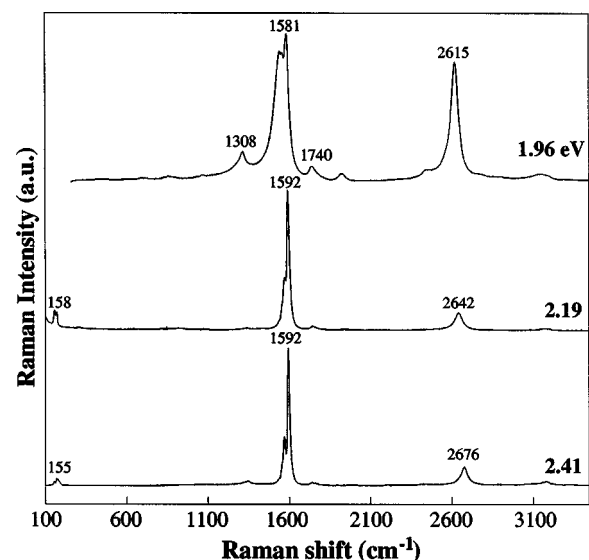


FIG. 1. First- and second-order Raman spectra for carbon nanotubes over the broad phonon frequency range 100–3700 cm^{-1} for $E_{\text{laser}} = 1.96, 2.19,$ and 2.41 eV.

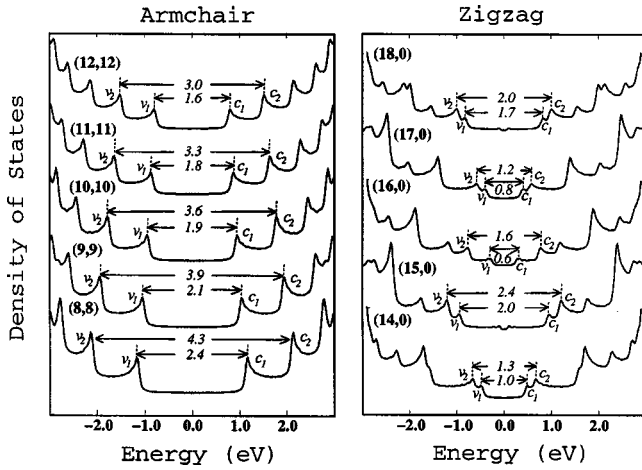


FIG. 2. Electronic 1D density of states (DOS) calculated with a tight binding model for (8,8), (9,9), (10,10), (11,11), and (12,12) armchair nanotubes and for (14,0), (15,0), (16,0), (17,0), and (18,0) zigzag nanotubes. (Ref. 5) Wave-vector conserving optical transitions can occur between mirror image singularities in the 1D density of electronic states of the valence and conduction bands, i.e., $v_1 \rightarrow c_1$ and $v_2 \rightarrow c_2$, etc. These optical transitions, which are given in the figure in units of eV and are denoted in the text by E_{11} , E_{22} , etc., are responsible for the resonant Raman effect. The 1D density of electronic states for chiral nanotubes (n,m) tends to be similar to the results shown here for the zigzag nanotubes. Metallic nanotubes require that $2n+m=3q$, where q is an integer. The DOS was calculated for $\gamma_0=3.0$ eV.

tween the i th conduction band singularity and the i th valence band singularity), $E_{ii}=E_{11}, E_{22}, \dots$, shown in Fig. 2. A summary of all the E_{ii} energy separations for all (n,m) nanotubes up to a nanotube diameter of 3.0 nm is given in Fig. 3. A similar figure was first published by Kataura *et al.*⁷ for $\gamma_0=2.75$ eV, but the plot presented here is for $\gamma_0=2.90$ eV,⁸ which provides a better fit to our Raman data. Resonant enhancement occurs not only for the incident photon but also for the scattered photon, so that the conditions for resonant Raman scattering include $E_{\text{laser}}=E_{ii}$ and $E_{\text{laser}}=E_{ii}+\hbar\omega_{\text{phonon}}$ for the Stokes process. The window for resonance Raman scattering for the incident and scattered light is shown in Fig. 3 for the 1.49 ± 0.20 nm diameter nanotubes used in the present measurements.

Figure 3 also shows that the electronic transition from the highest energy singularity in the valence band density of states to the lowest energy singularity in the conduction band density of states for the metallic nanotubes (open circles) at constant nanotube diameter $E_{11}^M(d_t)$ has a width, and this width is associated with trigonal warping effects⁸ arising from the noncircular constant energy surfaces that develop with increasing wave vector away from the K point in the Brillouin zone. This trigonal warping effect is most important for zigzag nanotubes (see Fig. 2) and least important for armchair tubes, for which a simple analytical expression for $E_{11}^M(d_t)$ can be written as

$$E_{11}^M(d_t) = 6a_{C-C}\gamma_0/d_t, \quad (1)$$

where a_{C-C} is the nearest neighbor carbon-carbon distance. It should be mentioned that Eq. (1) is only valid for chiral and zigzag nanotubes in the limit of large d_t .

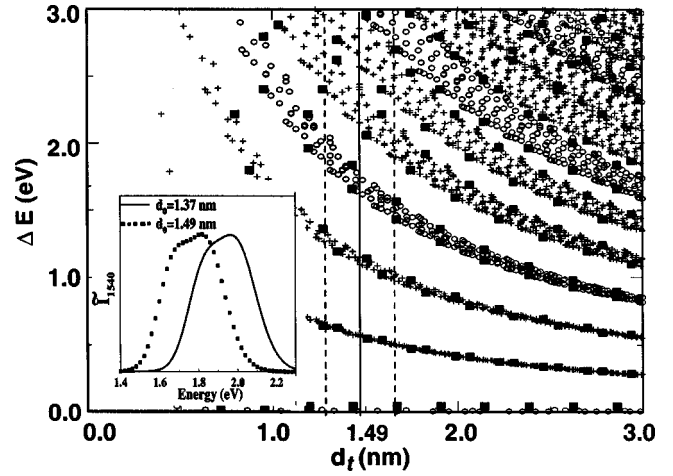


FIG. 3. Calculation of the energy separations $\Delta E=E_{ii}(d_t)$ for nanotubes with all (n,m) indices (Ref. 16) as a function of nanotube diameter in the range $0.7 < d_t < 3.0$ nm [based on prior work of Kataura *et al.* (Ref. 7)]. The calculation is based on the tight-binding model with $\gamma_0=2.90$ eV and $s=0$, where s is the tight-binding overlap integral. The semiconducting and metallic nanotubes are indicated by crosses and open circles, respectively. The filled squares denote the zigzag tubes. The inset shows the experimental range of E_{laser} , which is resonant with metallic nanotubes of diameters $d_t=1.49\pm 0.20$ nm (square points) and $d_t=1.37\pm 0.18$ nm (solid curve) (Ref. 2).

Since the energy separations $E_{ii}(d_t)$ in Figs. 2 and 3 are strongly dependent on the diameter d_t of the nanotubes, a change in the energy of the incident laser beam E_{laser} results in the resonant Raman excitation of *different* nanotubes. Furthermore, $\hbar\omega_{\text{phonon}}$ can be as large as 0.4 eV for second-order scattering processes for the tangential modes. Therefore, the specific nanotubes in a given sample that are excited in the first-order Raman scattering process are likely to be different from the nanotubes that participate in the second-order scattering process. In this paper, we also demonstrate the importance of the scattered photon in the second-order Raman spectra. Since the scattered photon propagates in all directions, it is expected to couple resonantly to more of the randomly oriented carbon nanotubes than the incident photon, which couples most strongly to nanotubes whose axes are aligned along the optical electric field of the incident beam. Thus the probability of an optical resonance with the scattered beam is expected to be higher than that for the incident beam.

Regarding the first-order spectrum, the radial breathing mode frequency ω_{RBM} for an isolated nanotube depends on the nanotube diameter d_t in accordance with $\omega_{\text{RBM}} \propto 1/d_t$, independent of the chirality of the nanotube. Therefore, a variation of E_{laser} results in a variation of the observed ω_{RBM} due to selective resonance with *different* nanotubes, as has been studied extensively by many authors.^{1,3,9-15} Since the radial breathing mode is observed in the second-order Raman spectrum as both a harmonic (overtone) and as a combination mode, the special resonant features of the radial breathing mode in the first-order spectrum associated with the 1D density of electronic states also affects the second-order spectrum in important ways, as discussed below.

The characteristic features of the tangential modes of the first-order spectrum are also due to resonant Raman effects

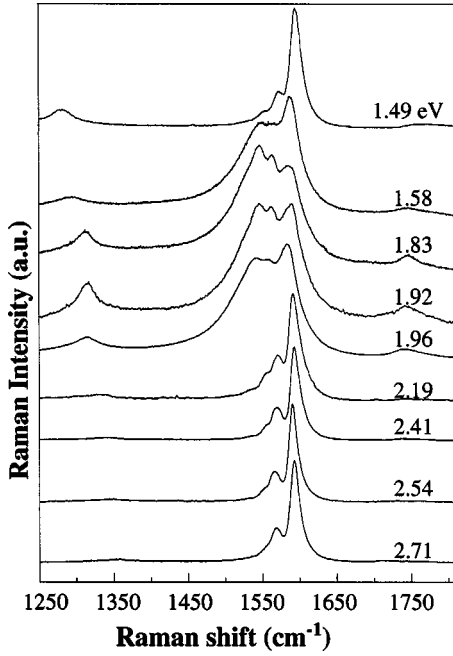


FIG. 4. First-order Raman spectra for the tangential mode ($1500\text{--}1650\text{ cm}^{-1}$) taken for nine laser excitation energies. At lower frequencies ($1300\text{--}1350\text{ cm}^{-1}$) the *D*-band feature is observed, and at higher frequencies near 1750 cm^{-1} a combination mode is seen for some values of E_{laser} .

associated with singularities in the 1D electron density of states, but the tangential mode spectra have characteristics that are different from those of the radial breathing modes. Results for the first-order resonant Raman spectra for the tangential modes for the sample used in the present study (diameter distribution $d_t = 1.49 \pm 0.20\text{ nm}$) are presented in Fig. 4 for nine different laser excitation energies. Since the tangential modes of single-wall carbon nanotubes have only a very weak dependence on nanotube diameter,^{3,16} the characteristic features of the Raman spectra for the tangential band over a wide range of E_{laser} in Fig. 4 ($E_{\text{laser}} = 1.49\text{ eV}$ and $2.19 \leq E_{\text{laser}} \leq 2.71\text{ eV}$) are essentially independent of E_{laser} .² However, in the range of $1.58 \leq E_{\text{laser}} \leq 1.96\text{ eV}$, additional features in the first-order resonant Raman spectra for the tangential band are observed. In addition, the Raman spectra for the range $1.58 \leq E_{\text{laser}} \leq 1.96\text{ eV}$ show extensive broadening. We attribute these additional features and the line broadening effects to laser-induced electronic resonances involving *metallic* nanotubes and to the coupling between phonons and conduction electrons in metallic nanotubes.² For the particular nanotube sample used in the present work, the diameter distribution is determined to be $d_t = 1.49 \pm 0.20\text{ nm}$ based on the proportionality constant calculated using the results of transmission electron microscopy (TEM) and Raman spectroscopy (ω_{RBM} for the radial breathing mode) measurements made at many E_{laser} values in the present study on the nanotubes used in Ref. 2 ($d_t = 1.37 \pm 0.18\text{ nm}$). Therefore, we infer that the nanotubes used in this study are $\sim 9\%$ larger. Consequently, the resonant energies for the metallic window for the 1.49-nm diameter sample are lowered with respect to that for the 1.37-nm diameter sample, as can be seen from the inset to Fig. 3, which gives a comparison between the metallic windows for the

TABLE I. A summary of the peak frequencies and linewidths (in cm^{-1}) of the main components of the tangential modes (ω_{tang}) (see Fig. 4) and their overtones ($2\omega_{\text{tang}}$) (see Fig. 6) of the single-wall carbon nanotubes, for selected values of E_{laser} .

E_{laser}	1.96 eV		2.19 eV		2.41 eV		2.71 eV	
Line	ω	γ	ω	γ	ω	γ	ω	γ
ω_{tang}								
no. 1	1515	50	—	—	—	—	—	—
no. 2	1540	44	—	—	—	—	—	—
no. 3	1564	27	1567	33	1567	18	1567	21
no. 4	1581	18	—	—	—	—	—	—
no. 5	1591	16	1592	9	1592	9	1592	11
no. 6	1601	36	1599	22	1599	18	1599	20
$2\omega_{\text{tang}}$								
no. 1	3082	87	—	—	—	—	—	—
no. 2	3122	55	3119	55	—	—	—	—
no. 3	3153	49	3150	49	3141	32	3153	32
no. 4	3178	40	3172	45	3166	47	3181	38
no. 5	3203	34	3201	38	3195	54	3216	51

two samples, plotted in terms of the normalized intensity of the dominant Lorentzian component for the metallic nanotubes \tilde{I}_{1540} vs E_{laser} discussed below. In both cases the fit to the metallic window of the nanotubes yielded a value of $\gamma_0 = 2.95 \pm 0.05\text{ eV}$, which is consistent with the values of γ_0 used in the calculations by Charlier⁵ for Fig. 2 (3.0 eV) and by Saito⁸ for Fig. 3 (2.9 eV). Therefore, the first-order resonant Raman spectra associated with the tangential modes for the 1.49-nm nanotube sample are somewhat different in detail from the spectra shown in Ref. 2 for the 1.37-nm nanotube sample. The first-order spectra presented in Fig. 4 are to be compared with the second-order spectra for the same sample, which are presented below.

A line-shape analysis of the spectra in Fig. 4 is reported here and a summary of the peak frequencies and linewidths of the main components of the first-order tangential band is given in Table I for four E_{laser} values. The results show that the same dominant Lorentzian components are found in the spectra taken at 2.19, 2.41, 2.54 (not shown in Table I), and 2.71 eV, showing similar peak frequencies, linewidths, and relative intensities. Also, three additional, intense broad components are found in the spectra for $E_{\text{laser}} = 1.58, 1.83, 1.92,$ and 1.96 eV (see Table I for the additional spectral components at $E_{\text{laser}} = 1.96\text{ eV}$). The broad features at 1515 cm^{-1} and 1540 cm^{-1} and the narrower feature at 1581 cm^{-1} are identified with metallic nanotubes.² For the 1.49-nm diameter sample, the normalized intensity of the feature at 1540 cm^{-1} associated with metallic nanotubes is a maximum for $E_{\text{laser}} \sim 1.8\text{ eV}$ (see inset to Fig. 3), and here the normalization of \tilde{I}_{1540} is done with respect to the intensity of the 1592-cm^{-1} feature, which is the most intense Lorentzian oscillator associated with semiconducting nanotubes.

Figure 4 also shows the presence of a Raman band near 1330 cm^{-1} , which occurs at about the same frequency as the *D* band in disordered and small crystallite size sp^2 carbons.

The D band in single-wall carbon nanotubes has a large dispersion in peak frequency as a function of E_{laser} , as well as a strong dependence of its intensity on E_{laser} . All sp^2 carbons (including both 2D and 3D structures) also exhibit a resonant second-order Raman band that is strongly dependent on E_{laser} and dominates the second-order spectrum.¹⁷ The physical origin of this resonant second-order Raman band, also called the G' band, has recently been explained in sp^2 carbons in terms of a strong coupling between electrons and phonons with the same wave vector in the vicinity of the K point of the 2D Brillouin zone, where the electronic energy bands exhibit unique linear k -dependent phonon and electron dispersion relations.¹⁷ Although the frequency of the G' band occurs at twice the frequency of the disorder-induced D band, the G' band is also observed with approximately equal intensity for highly crystalline graphite, which has no first-order D -band intensity.

Analogous resonant Raman phenomena occur for carbon nanotubes, giving rise to the most intense feature in the second-order Raman spectra in Fig. 1. This figure shows the relative intensity of the G' band feature to be very sensitive to E_{laser} for single-wall carbon nanotubes. All the nanotubes in the sample contribute resonantly to the G' -band feature at a given E_{laser} , thereby accounting for its high intensity. The laser excitation energy ($E_{\text{laser}}=1.96$ eV) in Fig. 1 where the intensity of the G' band is the largest is also the E_{laser} value where the D -band intensity is the largest. A detailed discussion of the special characteristics of the G' band and the D band in single-wall carbon nanotubes is presented elsewhere.⁴

II. EXPERIMENTAL DETAILS

The single-walled carbon nanotubes of the present study were synthesized by Carbolex Inc. of Lexington, Kentucky using a modified electric arc technique. A catalyst with a 4:1 Ni:Y atomic ratio was used in the nanotube synthesis. Second-order spectra were taken on several different Carbolex single-wall carbon nanotube samples, and results consistent with those reported here were obtained for each sample batch. The diameter distribution of these samples is 1.49 ± 0.20 nm.

Raman spectroscopy experiments were performed under ambient conditions in a backscattering configuration using several laser excitation lines. These lines include the argon lines at 457.9 nm (2.71 eV), 488 nm (2.54 eV) and 514.5 nm (2.41 eV); the krypton lines at 568.2 nm (2.19 eV), 647.1 nm (1.92 eV) and 676.4 nm (1.83 eV); the He-Ne line at 632.8 nm (1.96 eV); and a diode laser at 785 nm (1.58 eV). The spectral resolution of the different Raman systems for phonons was better than 2 cm^{-1} . A Ti:sapphire laser at 830 nm (1.49 eV) was also used, where the spectral resolution for this system was ~ 8 cm^{-1} .

III. EXPERIMENTAL RESULTS

We discuss below the various features in the second-order spectrum associated with the harmonics (overtones) and combination modes of the two dominant features of the first-order spectrum.

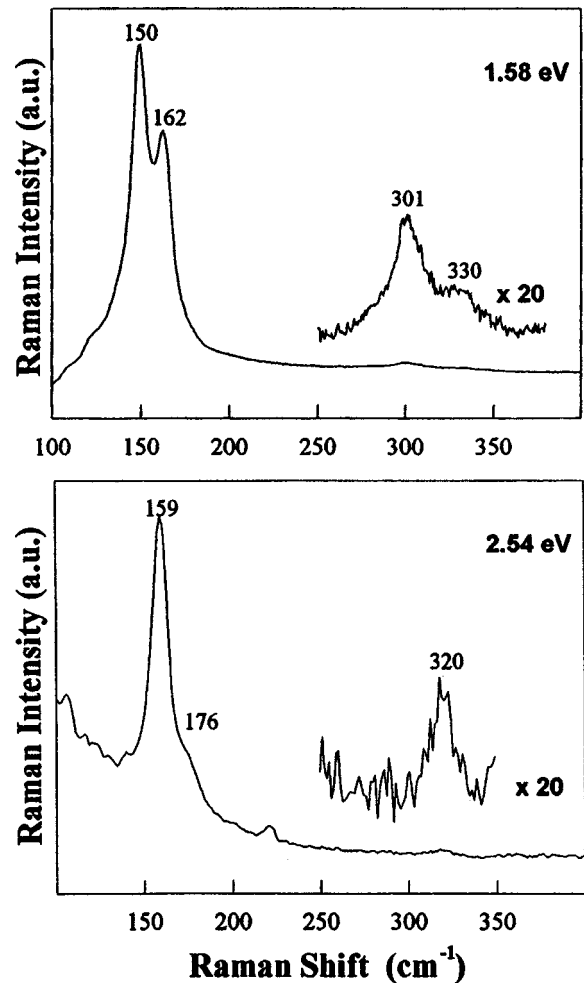


FIG. 5. The Raman spectra for the radial breathing mode band and its second harmonic at two laser excitation energies 1.58 eV (785 nm) and 2.54 eV (488 nm).

A. Overtones

In Fig. 5, we see spectral features identified with the second harmonic (overtone) of the radial breathing mode $2\omega_{\text{RBM}}$ at two different laser excitation energies. For example, at $E_{\text{laser}}=1.58$ eV (785 nm), the first-order spectrum gives resonantly enhanced radial breathing modes at 150 cm^{-1} and 162 cm^{-1} , with linewidths [full width at half maximum (FWHM)] of 14 cm^{-1} and 11 cm^{-1} , respectively, to be compared with the second-order lines which occur at 301 cm^{-1} and 330 cm^{-1} and have relatively narrow linewidths (21 cm^{-1}). A change in E_{laser} excites different nanotubes, so that for $E_{\text{laser}}=2.54$ eV (488 nm), the first-order Raman spectrum shows a radial breathing mode at 159 cm^{-1} and a small shoulder at 176 cm^{-1} . The second harmonic of this first-order band shows a weak second-order feature at 320 cm^{-1} (see Fig. 5). Similar trends are observed at other values of E_{laser} . The intensity of the overtone of the radial breathing mode is especially strong for E_{laser} values where contributions from metallic nanotubes dominate the spectra for the tangential band (see Fig. 4). A summary of our observations of the overtones of the radial breathing mode is given in Table II.

In contrast, the second harmonic of the tangential band $2\omega_{\text{tang}}$, which occurs in the range 3100 – 3250 cm^{-1} (see

TABLE II. Summary of the peak frequencies and linewidths (in cm^{-1}) of the Lorentzian components for the radial breathing modes (ω_{RBM}) and their overtones ($2\omega_{\text{RBM}}$) for the indicated E_{laser} values (see Fig. 5).

E_{laser}	1.58 eV		2.19 eV		2.41 eV		2.54 eV	
Line	ω	γ	ω	γ	ω	γ	ω	γ
ω_{RBM}								
no. 1	—	—	—	—	142	10	—	—
no. 2	150	14	—	—	155	10	—	—
no. 3	162	11	158	10	—	—	159	11
no. 4	—	—	171	10	170	10	—	—
no. 5	—	—	—	—	178	10	176	9
no. 6	—	—	—	—	188	10	—	—
$2\omega_{\text{RBM}}$								
no. 1	301	20	—	—	—	—	—	—
no. 2	—	—	311	30	—	—	—	—
no. 3	—	—	—	—	—	—	320	15
no. 4	330	20	—	—	—	—	—	—

Fig. 6), has very different characteristics from the second harmonic of the radial breathing mode $2\omega_{\text{RBM}}$ shown in Fig. 5. We see in Fig. 6 the evolution with E_{laser} of the second harmonic of the tangential band for five laser energies in the range 1.96–2.71 eV. The central frequency and linewidth of this second-order band are relatively weakly dependent on E_{laser} for $2.19 < E_{\text{laser}} \leq 2.71$ eV, where the semiconducting nanotubes dominate the first-order spectra for this sample. However, for $E_{\text{laser}} = 1.96$ eV, where the dominant contribution to the first-order spectrum in Fig. 4 comes from metallic nanotubes, the second-order spectrum is downshifted and much broader than for the higher E_{laser} values, consistent with the behavior of the first-order tangential band shown in Fig. 4.

The feature in the second-order Raman spectrum for graphite near 3240 cm^{-1} is strongly affected by the mode frequency dispersion of the phonon dispersion curves.^{18,19} This mode frequency dispersion in graphite gives rise to a peak in the phonon density of states near 1620 cm^{-1} , associated with non-zone-center phonons. This peak in the phonon density of states is responsible for the feature in the second-order spectrum of graphite near 3240 cm^{-1} . This frequency is upshifted by 76 cm^{-1} from twice the zone-center phonon mode in graphite at 1582 cm^{-1} . Since there is no corresponding peak in the density of states away from the Brillouin zone center in carbon nanotubes, we expect the mode frequency of the second-order tangential band to be close to twice that for the first-order tangential band, consistent with experiment.

Even though the tangential band for carbon nanotubes contains modes with different symmetry types, the second harmonic of any irreducible representation always contains the completely symmetric irreducible representation A_g in the direct product of $\Gamma_i \otimes \Gamma_i$. Thus second harmonics of modes that are not Raman-active in the first-order spectrum could become Raman-active in the second-order spectrum

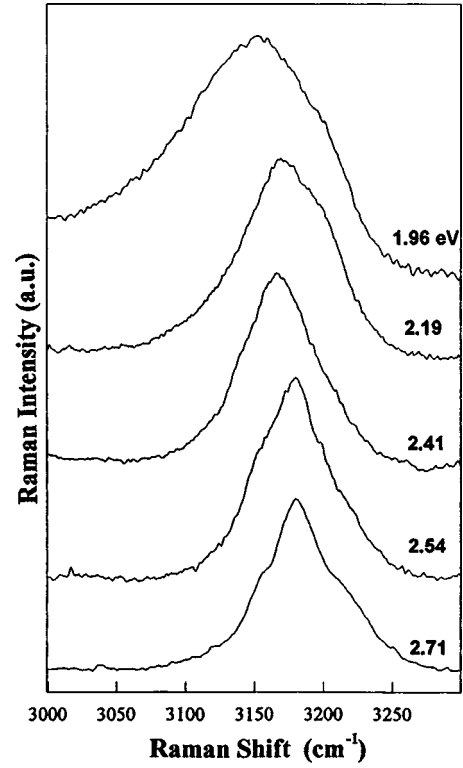


FIG. 6. Raman spectra for the second harmonic of the tangential mode, collected at five laser excitation energies. The corresponding first-order spectra are displayed in Fig. 4.

through this direct product argument. However, the intensity of such new modes in the second-order spectra is expected to be low.

A Lorentzian line-shape analysis of the second-order spectrum associated with the second harmonic of the tangential band has been carried out for the spectra shown in Fig. 6, and the results are presented in Table I. Two examples of this line-shape analysis are shown in Fig. 7. Here we present the line-shape analysis for the first-order and second-order features taken for E_{laser} at 2.71 eV, where the semiconducting nanotubes mainly contribute, and at 1.96 eV, where the metallic nanotubes mainly contribute.² The dominant feature in the 2.71-eV second-order spectrum at 3181 cm^{-1} is close to twice the frequency of the dominant mode in the first-order spectrum $2(1592) = 3184 \text{ cm}^{-1}$, and the second-order feature is only slightly broader than twice the FWHM linewidth of the first-order feature. The frequencies of the two weaker features in the second-order spectrum at 2.71 eV correspond approximately to twice the frequencies of the first-order features. As E_{laser} decreases from 2.71 eV, the peak frequency of the entire second-order band (see Fig. 6) downshifts, especially for the lowest value of E_{laser} , because new tangential peaks associated with metallic nanotubes are resonantly enhanced. For example, the second-order peaks in the 2.19-eV and 2.41-eV spectra are at 3171 cm^{-1} and 3166 cm^{-1} (see Table I), both downshifted relative to $2 \times 1592 = 3184 \text{ cm}^{-1}$. The second-order spectrum at $E_{\text{laser}} = 1.96$ eV in Fig. 6 shows a broad, asymmetric band with more scattering intensity at low phonon frequencies. Analysis of the line-shape of this Raman band in Fig. 7 shows a feature at 3082 cm^{-1} , which is close to $2 \times 1540 \text{ cm}^{-1}$, thereby providing

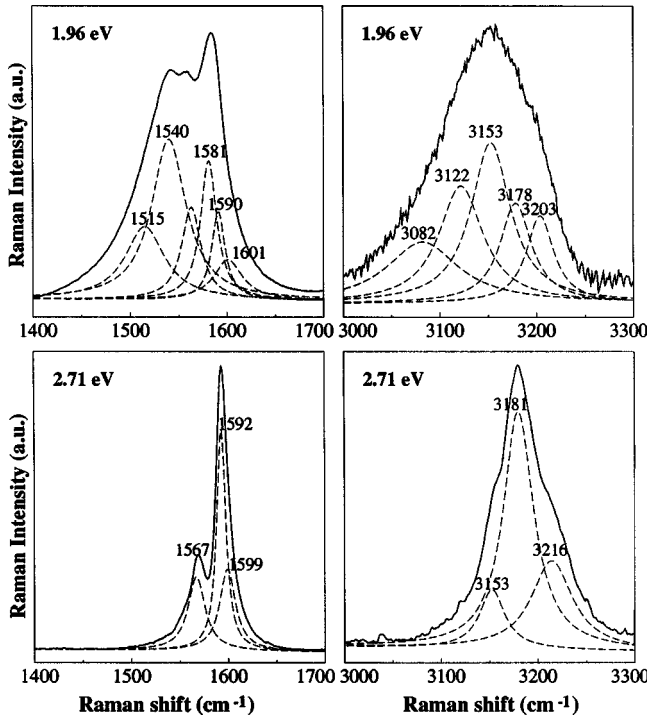


FIG. 7. A line-shape analysis of the spectral features in the first-order spectra (left) and in the second-order spectra (right) for the tangential bands taken for $E_{\text{laser}} = 1.96$ eV (632.8 nm) and 2.71 eV (457.9 nm).

support for the interpretation that metallic nanotubes are contributing to this second-order Raman band at $E_{\text{laser}} = 1.96$ eV.

Shown in Fig. 8 is an increase in linewidth, measured as the full width at half maximum intensity (FWHM), of the entire second-order band with decreasing E_{laser} . In this figure the increase in linewidth for the entire second-order band is compared with that for the first-order band as a function of E_{laser} . The large linewidth below ~ 2.0 eV in the first-order spectra in Fig. 8(a) is associated with the large contribution to the spectral intensity from metallic nanotubes (see Fig. 4).² We note in Fig. 8(b) that the onset of the broadening of the second-order features extends to much higher values of E_{laser} , so that at $E_{\text{laser}} = 2.2$ eV (where the scattered photons are still within the metallic window for the second-order spectrum) the linewidth is ~ 17 cm^{-1} broader than at $E_{\text{laser}} = 2.71$ eV.

The resonant enhancement in the phonon modes for metallic nanotubes occurs when the energy of either the incident

or the scattered photon is in resonance with the first electronic transition E_{11}^M for the metallic nanotubes in the sample (see Figs. 2, 3, and 4). When $E_{\text{laser}} = 1.92$ eV and 1.96 eV, both the incident and scattered photons are in the resonance window for metallic nanotubes, so that the overtone band is expected to broaden considerably, and this is observed experimentally in Fig. 8(b). For $2.19 \text{ eV} \leq E_{\text{laser}} \leq 2.41$ eV, even though the incident photon is higher than the resonance energy window E_{laser} for metallic nanotubes in the first-order spectrum (see Fig. 4), the energy of the scattered photon falls within the interval of resonant enhancement for metallic nanotubes, because the phonon frequency of 3200 cm^{-1} in the Stokes process corresponds to a large energy upshift (~ 0.4 eV). This is evident by a broadening [Fig. 8(b)] and a downshift of the 3200-cm^{-1} band for $E_{\text{laser}} = 2.19$ eV and 2.41 eV (see Fig. 6 and Table I). Because of the large value for $\hbar\omega_{\text{phonon}}$, the specific nanotubes contributing to the first-order spectrum may be different from the nanotubes contributing to the second-order spectra at $E_{\text{laser}} = 2.19$ eV and 2.41 eV.

B. Combination Modes

Resonant Raman effects associated with the 1D electron density of states singularities also give rise to resonant effects in the combination modes. One clear example of a combination mode occurs at the sum frequency between a tangential and a radial breathing mode $\omega_{\text{tang}} + \omega_{\text{RBM}}$, as shown in the spectra in Fig. 9 taken at $E_{\text{laser}} = 1.58$ eV, 1.96 eV, 2.14 eV, and 2.71 eV. Since the radial breathing mode (ω_{RBM}) spectra at $E_{\text{laser}} = 1.58$ eV consist of two lines at 150 cm^{-1} and 162 cm^{-1} (see Fig. 5), then using the most intense line at 1591 cm^{-1} for the tangential band ω_{tang} yields a sum of 1741 cm^{-1} and 1753 cm^{-1} , in good agreement with the dominant peak at 1742 cm^{-1} and in fair agreement with the weak feature at 1761 cm^{-1} , obtained from a line-shape analysis of the combination mode feature shown in Fig. 9.

In Table III the mode frequencies and linewidths of the combination modes for the 1740-cm^{-1} band associated with the combination mode $\omega_{\text{tang}} + \omega_{\text{RBM}}$ are listed. The relative intensities of this combination mode at various values of E_{laser} are displayed in Fig. 4 where it is seen that this feature is most prominent near ~ 1.8 eV where the metallic tube contribution is dominant for single-wall nanotubes for which $d_t \sim 1.49$ nm. Since the tangential mode frequency ω_{tang} is expected to be almost independent of E_{laser} , while the radial breathing mode frequency varies as $\omega_{\text{RBM}} \propto 1/d_t$, the shifts in

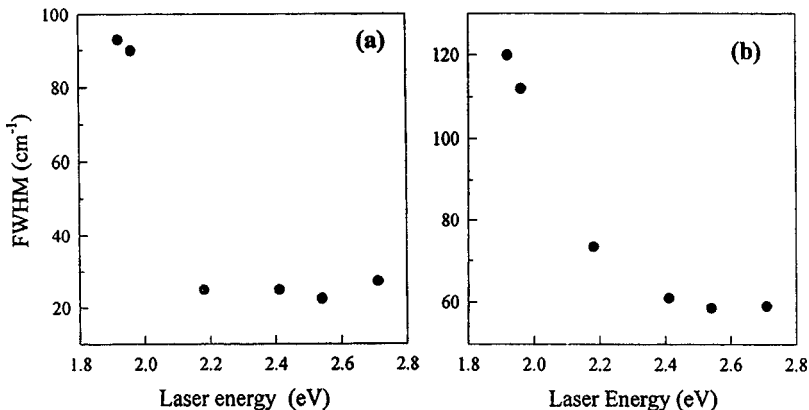


FIG. 8. Linewidth (FWHM) as a function of E_{laser} (a) for the entire first-order tangential band and (b) for the corresponding entire second harmonic of the tangential band.

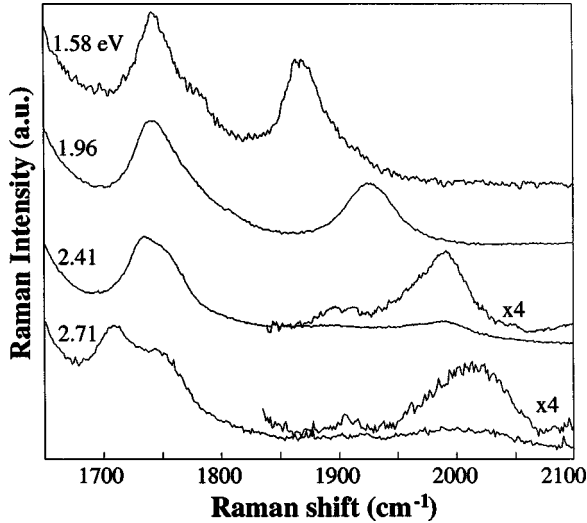


FIG. 9. Spectral features tentatively associated with combination bands for $\omega_{\text{tang}} + \omega_{\text{RBM}}$ and $\omega_{\text{tang}} + 2\omega_{\text{RBM}}$ in the second-order Raman spectra of carbon nanotubes at $E_{\text{laser}} = 1.58$ eV (785 nm), 1.96 eV (632.8 nm), 2.41 eV (514.5 nm), and 2.71 eV (457.9 nm).

the peaks of the 1740- cm^{-1} band for various E_{laser} lines are expected to reflect the variation in ω_{RBM} as E_{laser} is varied, since different nanotubes are resonantly excited at each value of E_{laser} . Since $\hbar\omega_{\text{phonon}} \sim 0.2$ eV for this combination mode, it is also possible that at a given value of E_{laser} different nanotubes within the sample are resonantly enhanced in the first-order spectrum as compared with the second-order spectrum.

The spectra in Fig. 9 show the feature that we tentatively assign to the combination mode $\omega_{\text{tang}} + \omega_{\text{RBM}}$ (~ 1740 cm^{-1}) has a similar peak position and linewidth for $E_{\text{laser}} = 1.58$ eV and 1.96 eV in the metallic regime. We note that the linewidth of this mode increases with increasing E_{laser} above 2.4 eV. The broad line observed for $E_{\text{laser}} = 2.41$ eV could in part be attributed to the excitation of many nanotubes for this value of E_{laser} , as suggested by the radial breathing mode spectrum at 2.41 eV (see Table II). However, the Raman spectra taken at 2.54 eV (not shown) and at 2.71 eV (see Fig. 9) show further broadening of this combination mode, a decrease in mode intensity, and the development of a doublet structure. For $E_{\text{laser}} = 2.54$ eV, there are relatively few radial breathing mode peaks in the first-order spectrum. The analysis in Table III shows that the frequency of the two components of the $\omega_{\text{tang}} + \omega_{\text{RBM}}$ feature both downshift as E_{laser} increases, though the downshift is larger for the lower frequency component than it is for the upper frequency component. At this time, we have no good explanation for the mode splitting or for the downshifts in the mode frequencies of the $\omega_{\text{tang}} + \omega_{\text{RBM}}$ feature for $E_{\text{laser}} \geq 2.41$ eV.

In Fig. 9 we see another feature at higher frequencies that we tentatively assign to a second combination band, this one associated with $\omega_{\text{tang}} + 2\omega_{\text{RBM}}$. As shown in Fig. 9, this feature has a curious dependence on E_{laser} . While the combination band is located near 1870 cm^{-1} for $E_{\text{laser}} \sim 1.58$ eV (785 nm), the feature upshifts to ~ 1925 cm^{-1} for $1.83 < E_{\text{laser}} < 2.19$ eV, and then upshifts again to ~ 2000 cm^{-1} for $2.41 < E_{\text{laser}} < 2.71$ eV (see Fig. 9 and Table II). If we assume

TABLE III. Summary of the peak frequencies and linewidths (in cm^{-1}) of the Lorentzian components for the combination modes tentatively identified with $\omega_{\text{tang}} + \omega_{\text{RBM}}$ and $\omega_{\text{tang}} + 2\omega_{\text{RBM}}$ for the combination bands in the range 1700–2000 cm^{-1} near 1900 cm^{-1} in Fig. 10 for five values of E_{laser} .

E_{laser}	1.58 eV		1.96 eV		2.41 eV		2.54 eV		2.71 eV	
	ω	γ								
$\omega_{\text{tang}} + \omega_{\text{RBM}}$										
	1737	32	1740	31	1733	30	1722	46	1710	39
	1762	50	1761	57	1756	34	1753	45	1750	37
$\omega_{\text{tang}} + 2\omega_{\text{RBM}}$										
	1871	31	1925	47	1990	52	2000	60	2011	62

$\omega_{\text{tang}} = 1590$ cm^{-1} and $\omega_{\text{RBM}} = 165$ cm^{-1} , then we get $\omega_{\text{tang}} + 2\omega_{\text{RBM}} = 1920$ cm^{-1} , which accounts for the frequency of the observed features for $1.83 \leq E_{\text{laser}} < 2.19$ eV. Weak features in the range 1900–1920 cm^{-1} can be observed also in the spectra at 2.41 eV and 2.71 eV. If we now assume that mostly metallic nanotubes dominate the spectrum for $E_{\text{laser}} = 1.58$ eV, then $\omega_{\text{tang}} = 1540$ cm^{-1} becomes a dominant feature in the first-order spectrum (see Fig. 7), leading to $\omega_{\text{tang}} + 2\omega_{\text{RBM}} = 1870$ cm^{-1} , which accounts nicely for the observations at $E_{\text{laser}} = 1.58$ eV. For $E_{\text{laser}} > 2.4$ eV where the intensity of this spectral feature becomes low, a new feature in the frequency range 1990–2010 cm^{-1} appears, as shown in Fig. 9. We have no further explanation for the dispersive effect that occurs for this feature with increasing E_{laser} above 2.41 eV.

C. 2D resonance phenomena

The most intense feature in the second-order spectrum (see Fig. 1) is the peak located at ~ 2680 cm^{-1} and this feature has an especially strong intensity near $E_{\text{laser}} = 1.96$ eV (Fig. 1). This feature, which is closely related to the G' feature in sp^2 carbons, shows a strong upshift in frequency as E_{laser} increases (see Fig. 10), which is more explicitly demonstrated in the plot of the peak frequencies versus E_{laser} given in the inset to Fig. 10. The large dispersion for sp^2 carbons is explained by resonance with electronic interband transitions near the K point in the 2D Brillouin zone, but for carbon nanotubes we have only a few allowed wave vectors in the circumferential direction of the nanotube. For all frequencies shown in the figure, the line-shape is fitted by a single Lorentzian component, with a linewidth that has a very weak dependence on E_{laser} . Assuming that the frequency of the G' band depends linearly on E_{laser} , consistent with the behavior of the G' band in other sp^2 carbons, the experimental G' -band frequencies for the sample in the present work extrapolate to 2429 cm^{-1} at $E_{\text{laser}} = 0$, and this phonon frequency is approximately twice the K -point phonon frequency in the 2D Brillouin zone of sp^2 carbons. This extrapolation agrees quite well with the direct measurement of this same phonon frequency (2440–2445 cm^{-1}), shown in Fig. 11.

The weak feature that appears at 2440 cm^{-1} in the second-order Raman spectrum of 2D graphite and other dis-

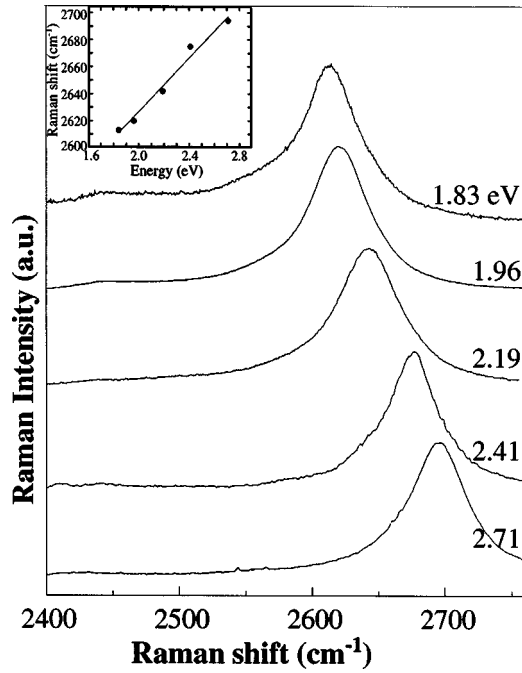


FIG. 10. The Raman spectra for the intense G' band for five values of E_{laser} . The inset shows a plot of the peak Raman frequency for the G' -band features vs laser excitation energy E_{laser} .

ordered carbons has been attributed to the sum of two K -point phonons, which each have a frequency of $\sim 1220 \text{ cm}^{-1}$ based on analysis of the 2D resonant Raman effect for the D band in sp^2 carbons.¹⁷ The phonon density of states in graphite shows a weak peak associated with these K -point phonons where an optical and an acoustic branch of the phonon spectrum for 2D graphite are degenerate at the zone edge K point. The K -point feature that appears in the phonon spectrum of graphite and disordered carbons is nonresonant, because the valence and conduction bands in the electronic structure are degenerate at the K point in the Brillouin zone and the photon that would be necessary to be in resonance with this phonon therefore has $E_{\text{laser}} \approx 0$.

For $E_{\text{laser}} = 1.83 \text{ eV}$, 1.92 eV , and 1.96 eV , the spectra in Fig. 11 show that the peak frequency and linewidth of the second harmonic (overtone) of the K -point phonon band are independent of E_{laser} , though at higher values of $E_{\text{laser}} = 2.41, 2.54$, and 2.71 eV , the peak downshifts, broadens, and becomes more asymmetric. Further insight into these observations is provided by looking at the energies of the scattered light. For $1.83 < E_{\text{laser}} < 1.96 \text{ eV}$, the energy of the scattered photon is between 1.50 eV and 1.66 eV , using a value of 2444 cm^{-1} for the K -point phonon in Fig. 11. For scattered photons in the range 1.53 eV to 1.66 eV , Fig. 3 shows that resonance with metallic nanotubes occurs. However, when $E_{\text{laser}} \geq 2.41 \text{ eV}$, the scattered phonons have energy $> 2.11 \text{ eV}$, which Fig. 3 shows to be outside the metallic window, so that only semiconducting nanotubes are excited. Figure 11 shows that the anomalous downshift in the K -point frequency occurs for laser energies that excite semiconducting nanotube phonons resonantly. We have no explanation at this time for the frequency downshift observed for $E_{\text{laser}} \geq 2.41 \text{ eV}$ in Fig. 11. However, it should be mentioned that the downshift of the $\omega_{\text{tang}} + \omega_{\text{RBM}}$ combination band, the upshift of the $\omega_{\text{tang}} + 2\omega_{\text{RBM}}$ combination band, and the down-

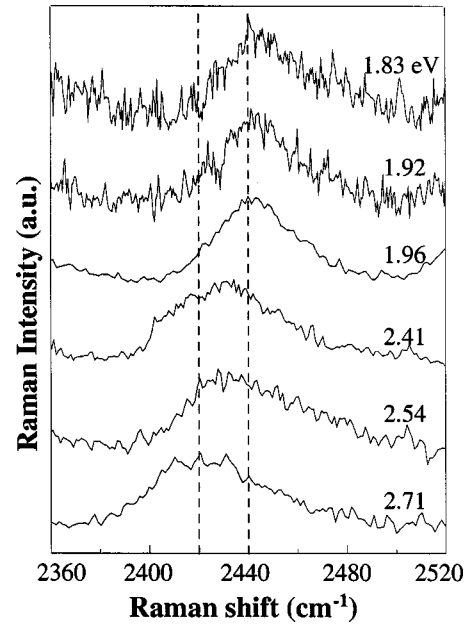


FIG. 11. The weak nonresonant feature associated with the second harmonic (overtone) of the K -point phonon in the 2D Brillouin zone for six values of E_{laser} . Dashed vertical lines are drawn at 2420 and 2440 cm^{-1} to illustrate the downshift of the K -point feature with increasing E_{laser} .

shift of the $2\omega_K$ point band all occur for $E_{\text{laser}} > 2.4 \text{ eV}$, suggesting a possible coupling between the combination bands and the overtone mode of the K -point phonons.

IV. CONCLUSIONS

Overtones and combination modes have been identified in the second-order spectra for the two dominant features in the first-order spectra (the radial breathing mode and the tangential mode) that are associated with the resonant Raman enhancement process arising from the 1D electronic density of states. Just as for the case of the first-order spectra, the resonant contributions to the second-order spectra also involve a different set of (n, m) nanotubes at each laser excitation energy E_{laser} . A second-order analog is observed for the broad spectral band identified with contributions from metallic nanotubes to the first-order tangential mode spectra. The unique feature of the second-order tangential overtone band shows a larger E_{laser} range over which the metallic nanotubes contribute. This effect is attributed to the large ($\hbar\omega_{\text{phonon}} \sim 0.4 \text{ eV}$) energy of these phonons and can be explained within the framework of the energy dependence of the electronic 1D density of states. Combination modes associated with $(\omega_{\text{tang}} + \omega_{\text{RBM}})$ and $(\omega_{\text{tang}} + 2\omega_{\text{RBM}})$ have been tentatively identified, and show behaviors as a function of E_{laser} that are consistent with the behavior of their first-order constituents, namely, that different nanotubes contribute to the spectra at each value of E_{laser} .

ACKNOWLEDGMENTS

The authors are thankful to Professor R. Saito for discussions about dispersion relations for electrons and phonons

and to Dr. Gene Hanlon for his help with the measurements. We gratefully acknowledge support for this work under NSF Grant No. DMR 98-04734. M.A.P. acknowledges support by the Brazilian agencies FAPEMIG, CAPES, and FINEP. P.C.

acknowledges support by the Brazilian agency FAPESP. The measurements performed at the George R. Harrison Spectroscopy Laboratory at MIT were supported by NIH Grant No. P41-RR02594 and NSF Grant No. CHE9708265.

-
- ¹A.M. Rao, E. Richter, S. Bandow, B. Chase, P.C. Eklund, K.W. Williams, M. Menon, K.R. Subbaswamy, A. Thess, R.E. Smalley, G. Dresselhaus, and M.S. Dresselhaus, *Science* **275**, 187 (1997).
- ²M.A. Pimenta, A. Marucci, S. Empedocles, M. Bawendi, E.B. Hanlon, A.M. Rao, P.C. Eklund, R.E. Smalley, G. Dresselhaus, and M.S. Dresselhaus, *Phys. Rev. B* **58**, R16 016 (1998).
- ³M. S. Dresselhaus, G. Dresselhaus, M. A. Pimenta, and P. C. Eklund, *Analytical Applications of Raman Spectroscopy* (Blackwell Science, Oxford, UK, 1999), pp. 367–434.
- ⁴M. A. Pimenta, E. B. Hanlon, A. Marucci, P. Corio, S. D. M. Brown, S. Empedocles, M. Bawendi, G. Dresselhaus, and M. S. Dresselhaus (unpublished).
- ⁵J.-C. Charlier (private communication).
- ⁶M. S. Dresselhaus, G. Dresselhaus, K. Sugihara, I. L. Spain, and H. A. Goldberg, *Graphite Fibers and Filaments*, Springer Series in Materials Science Vol. 5 (Springer-Verlag, Berlin, 1988).
- ⁷H. Kataura, Y. Kumazawa, Y. Maniwa, I. Umezu, S. Suzuki, Y. Ohtsuka, and Y. Achiba, *Synth. Met.* **103**, 2555 (1999).
- ⁸R. Saito (private communication).
- ⁹C. Journet, W.K. Maser, P. Bernier, A. Loiseau, M. Lamy de la Chapelle, S. Lefrant, P. Deniard, R. Lee, and J.E. Fischer, *Nature* (London) **388**, 756 (1997).
- ¹⁰Y. Saito, Y. Tani, N. Miyagawa, K. Mitsushima, A. Kasuya, and Y. Nishina, *Chem. Phys. Lett.* **294**, 593 (1998).
- ¹¹M. Sugano, A. Kasuya, K. Tohji, Y. Saito, and Y. Nishina, *Chem. Phys. Lett.* **292**, 575 (1998).
- ¹²H. Kuzmany, B. Burger, M. Hulman, J. Kurti, A.G. Rinzler, and R.E. Smalley, *Europhys. Lett.* **44**, 518 (1998).
- ¹³A. Kasuya, M. Sugano, Y. Sasaki, T. Maeda, Y. Saito, K. Tohji, H. Takahashi, Y. Sasaki, M. Fukushima, Y. Nishina, and C. Horie, *Phys. Rev. B* **57**, 4999 (1998).
- ¹⁴E. Anglaret, N. Bendiab, T. Guillard, C. Journet, G. Flamant, D. Laplaze, P. Bernier, and J.L. Sauvajol, *Carbon* **36**, 1815 (1998).
- ¹⁵H. Kuzmany, B. Burger, A. Thess, and R.E. Smalley, *Carbon* **36**, 709 (1998).
- ¹⁶M. S. Dresselhaus, G. Dresselhaus, and P. C. Eklund, *Science of Fullerenes and Carbon Nanotubes* (Academic Press, New York, 1996); R. Saito, G. Dresselhaus, and M. S. Dresselhaus, *Physical Properties of Carbon Nanotubes* (Imperial College Press, London, 1998).
- ¹⁷M.J. Matthews, M.A. Pimenta, G. Dresselhaus, M.S. Dresselhaus, and M. Endo, *Phys. Rev. B* **59**, R6585 (1999).
- ¹⁸M. S. Dresselhaus, P. C. Eklund, and M. A. Pimenta, in *Raman Scattering in Materials Science*, edited by W. Weber and R. Merlin (Springer-Verlag, Berlin, in press).
- ¹⁹P.C. Eklund, J.M. Holden, and R.A. Jishi, *Carbon* **33**, 959 (1995).